Interaction Notes

Note 314

August 1976

EMP Penetration Through Metal Skin Panels and Into Aircraft Cavities

G. Bedrosian and K.S.H. Lee
The Dikewood Corporation, Westwood Research Branch
Los Angeles, California 90024

Abstract

This report examines EMP diffusion penetration through metal skin panels and into metallic cavities. The diffusion approximation of Kaden, valid in the limit that displacement currents can be neglected, is used to find for four canonical geometries (single and parallel plates, cylindrical shell, spherical shell) the frequency-domain transfer function, which is the ratio of the internal magnetic field to the uniform part of the external magnetic field. The resulting transfer functions can be inverse Laplace transformed to give the time-domain EMP responses for the four canonical geometries. Simple approximation formulas are derived for non-ferromagnetic, metallic cavities of arbitrary shape, for which the skin panel thickness is small compared to the volume-to-surface ratio, which allow accurate estimation of the time response of the interior magnetic field.

ACKNOWLEDGMENT

The authors are indebted to Drs. K. C. Chen, J. P. Castillo, and C. E. Baum of the Air Force Weapons Laboratory for enlightening discussions concerning the subject matter of the report.

Interaction Notes

Note 314

August 1976

EMP Penetration Through Metal Skin Panels and Into Aircraft Cavities

G. Bedrosian and K.S.H. Lee
The Dikewood Corporation, Westwood Research Branch
Los Angeles, California 90024

Abstract

This report examines EMP diffusion penetration through metal skin panels and into metallic cavities. The diffusion approximation of Kaden, valid in the limit that displacement currents can be neglected, is used to find for four canonical geometries (single and parallel plates, cylindrical shell, spherical shell) the frequency-domain transfer function, which is the ratio of the internal magnetic field to the uniform part of the external magnetic field. The resulting transfer functions can be inverse Laplace transformed to give the time-domain EMP responses for the four canonical geometries. Simple approximation formulas are derived for non-ferromagnetic, metallic cavities of arbitrary shape, for which the skin panel thickness is small compared to the volume-to-surface ratio, which allow accurate estimation of the time response of the interior magnetic field.

ACKNOWLEDGMENT

The authors are indebted to Drs. K. C. Chen, J. P. Castillo, and C. E. Baum of the Air Force Weapons Laboratory for enlightening discussions concerning the subject matter of the report.

TABLE OF CONTENTS

LIST OF ILLUSTRATIONS

LIST OF TABLES

I. INTRODUCTION

This report deals with EMP penetration through metal skin panels and into metallic cavities via the mechanism of diffusion. Generally, there are three different modes for EMP penetration into cavities: diffusion through the wall; inadvertent penetration through apertures such as seams, joints, and windows; and deliberate penetration through antennas. It is generally assumed that penetration due to diffusion will be completely dominated by inadvertent penetration through apertures and by deliberate penetration through antennas, but there are currently no simple, yet accurate, engineering formulas to provide a quantitative demonstration of this physically plausible assumption for specific aircraft cavities of interest, such as avionics bays, cockpit cavities, and weapons bays. It is the purpose of this report to present a set of simple working formulas for making an engineering estimate of EMP diffusion into a large class of metallic cavities.

It is virtually impossible to obtain an exact analytical solution of the appropriate boundary-value problem in the case of a metallic cavity of arbitrary shape, either in the time domain or in the frequency domain. However, there are several simplified cases which allow an exact solution. The one-dimensional problem of electromagnetic scattering from a zone occupied by a number of homogeneous regions separated by sharp discontinuities in electromagnetic parameters can be solved by matching at the boundaries solutions in each region, or, equivalently, by Ambarzumian's principle of invariance [ref. 1]. A "one-dimensional" problem can be a problem in which the only variation is along the z-axis in Cartesian coordinates (x,y,z), the ρ-axis in cylindrical coordinates (ρ,ϕ,z), or the r-axis in spherical coordinates (r,θ,ϕ). Accordingly, the "canonical" geometries are single and parallel plates, cylindrical shells, and spherical shells. The ratio of the magnetic field inside a canonical enclosure to the uniform part of the time-harmonic external magnetic field can be calculated using the diffusion approximation of Kaden [ref. 2]. The solutions derived by Kaden's method agree with the exact solutions when displacement currents are neglected [ref. 3]. The frequency-domain (time-harmonic)

solutions for the canonical geometries can be inverse Laplace transformed to the time domain. The resulting time-domain expressions are the basis for simple engineering formulas which give the interior magnetic field produced by an external EMP. For a typical high-altitude EMP and for typical aircraft metal skin panels (aluminum or titanium), the EMP can be treated as an impulse, as will be shown in this report.

There remains the problem of applying the canonical results to cases of practical interest. When the cavity walls are thin as compared to a typical length in the cavity, which is in turn smaller than the wavelengths of interest, the geometry dependence of the interior magnetic field is determined completely by the volume-to-surface ratio. By physical reasoning, the volume-to-surface ratio can be related to an effective inductance for the currents induced on the cavity wall. This observation leads to simple engineering estimates of the interior magnetic field produced by an external EMP for a large class of cavities onboard an aircraft.

In a separate report [ref. 4] numerical results will be presented for a typical high-altitude EMP incident on five aircraft cavities: the B-1 weapons bay, the B-1 central avionics bay, the EC-135 cockpit, the EC-135 fuselage, and the E-4 cockpit. The ease of application of the engineering formulas used to obtain these results invites further calculations for many other interesting cases.

II. METHOD OF SOLUTION

A. Frequency-Domain Solution

The transfer function, $\eta(s)$, is defined to be the ratio of the internal magnetic field (H^{int}) to the uniform part of the external magnetic field (H^{ext}):

$$\eta(s) = H^{int}(s)/H^{ext}(s) \qquad (s \equiv j\omega \equiv 2\pi jf)$$

Closely related to the transfer function is the shielding effectiveness, $S(s)$, where

$$S(s) = -20 \log_{10}|\eta(s)| \qquad \text{(in db)}$$

The following results are obtained for the canonical geometries using Kaden's diffusion approximation [ref 2]:

$$1/\eta(s) = \cosh(st_\Delta)^{\frac{1}{2}} + (Z_o/R)(st_\Delta)^{-\frac{1}{2}}\sinh(st_\Delta)^{\frac{1}{2}} \qquad (1)$$

for a single plate (figure 1),

$$1/\eta(s) = \cosh(st_\Delta)^{\frac{1}{2}} + [\mu_o r/(\mu\Delta)](st_\Delta)^{-\frac{1}{2}}\sinh(st_\Delta)^{\frac{1}{2}} \qquad (2)$$

for two parallel plates (figure 2),

$$1/\eta(s) = \cosh(st_\Delta)^{\frac{1}{2}} + [\mu_o r/(2\mu\Delta)](st_\Delta)^{\frac{1}{2}}\sinh(st_\Delta)^{\frac{1}{2}} \qquad (3A)$$

for a cylindrical shell with a longitudinal $\underline{H}$ (figure 3a),

$$1/\eta(s) = \cosh(st_\Delta)^{\frac{1}{2}} + \{[\mu_o r/(2\mu\Delta)](st_\Delta)^{\frac{1}{2}} + [\mu\Delta/(2\mu_o r)](st_\Delta)^{-\frac{1}{2}}\}\sinh(st_\Delta)^{\frac{1}{2}} \qquad (3B)$$

for a cylindrical shell with a transverse $\underline{H}$ (figure 3b) and, finally,

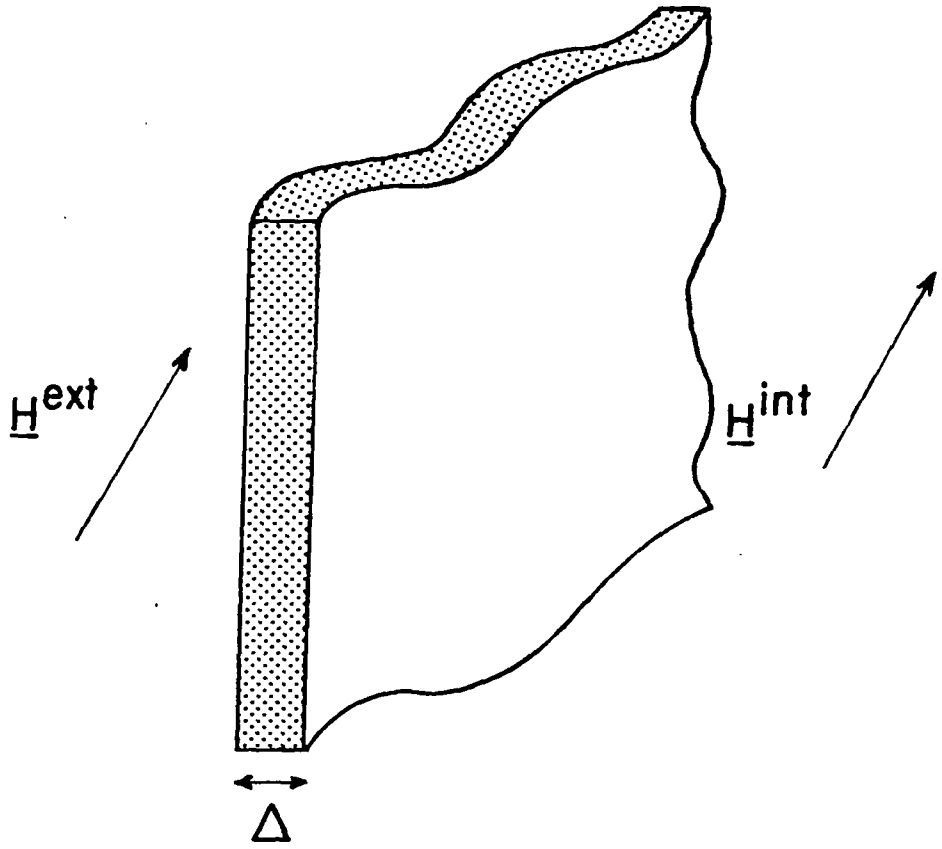

Figure 1. Shielding by a single plate with conductivity σ and permeability μ .

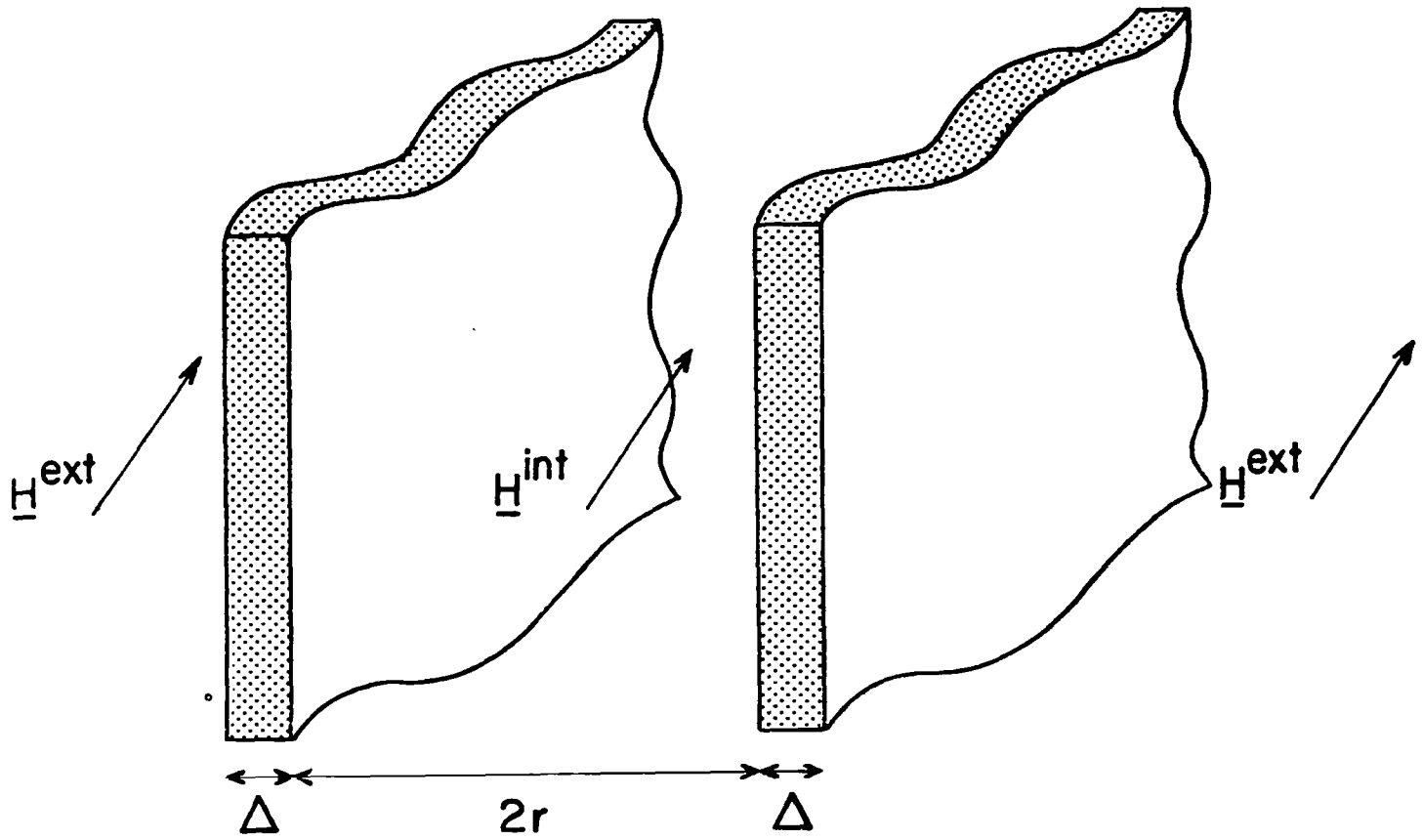

Figure 2. Shielding by two parallel plates with conductivity σ and permeability μ .

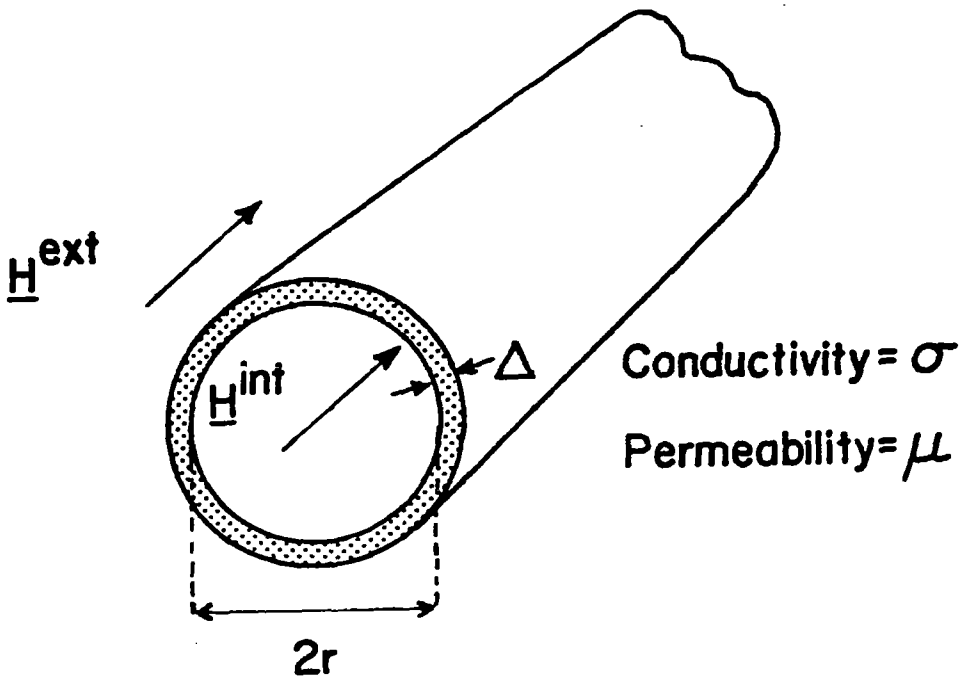

3(a)

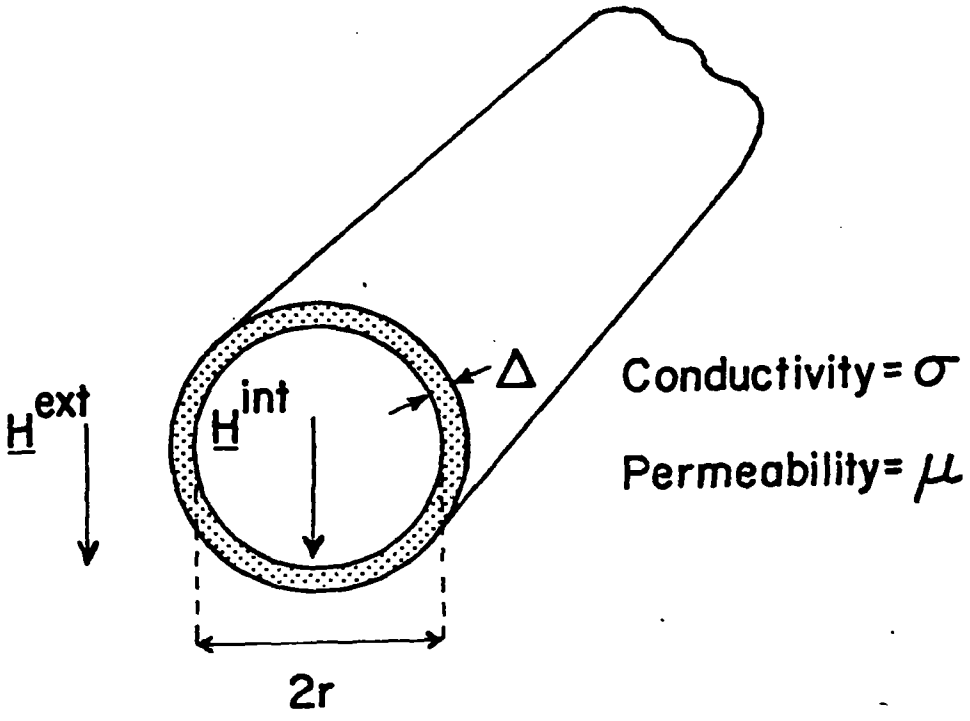

3(b)

Figure 3(a) - Shielding of a longitudinal magnetic field by an infinite cylindrical shell.

3(b) - Shielding of a transverse magnetic field by an infinite cylindrical shell.

$$1/\eta(s) = \cosh(st_\Delta)^{\frac{1}{2}} + \{[\mu_o r/(3\mu\Delta)](st_\Delta)^{\frac{1}{2}} + [2\mu\Delta/(3\mu_o r)](st_\Delta)^{-\frac{1}{2}}\}\sinh(st_\Delta)^{\frac{1}{2}} \quad (4)$$

for a spherical shell (figure 4), where

$Z_o = 377\ \Omega$ = impedance of free space

$\mu_o = 4\pi \times 10^{-7}$ henries per meter = permeability of free space

Δ = cavity wall thickness

σ = cavity wall conductivity

μ = cavity wall permeability

$R = (\sigma\Delta)^{-1}$ = D.C. resistance of cavity wall

$t_\Delta = \mu\sigma\Delta^2$ = diffusion time through the cavity wall

r = half plate separation (parallel plates) or radius (cylinder, sphere).

The shielding effectiveness and the magnitude of the transfer function of a single plate with $\Delta = 1.5$ mm (0.06") , $\mu = \mu_o$, and $\sigma = 2 \times 10^5$, 2.1×10^6 (titanium), 3.8×10^7 (aluminum), and 2×10^8 mhos per meter are plotted versus f in figures 5a and 5b. The parallel-plate shielding effectiveness and transfer function are plotted in figures 6a and 6b for $r = 1$ meter and Δ , μ , and σ as above. When the quantity, $\mu_o r/(\mu\Delta)$, is much greater than unity, the terms in $\eta(s)$ for the spherical and transverse cylindrical cases, which go as $\mu\Delta/(\mu_o r \sqrt{st_\Delta})$, have negligible effect. This is certainly the case for typical aircraft cavities, and so figures 6a and 6b can also be taken to apply to a cylinder of radius $r = 2$ meters (either polarization) or a sphere of radius $r = 3$ meters .

In figure 7, S is plotted versus f on an adjustable frequency scale for the enclosure cases. If ξ is defined to be the dimensionless coefficient of $(st_\Delta)^{\frac{1}{2}}\sinh(st_\Delta)^{\frac{1}{2}}$ in $\eta(s)$ for any of the enclosure geometires, then when s (or frequency, f) is small, the shielding effectiveness looks like

$$S \approx 20 \log_{10}|1 + 2\pi j\xi t_\Delta f|$$

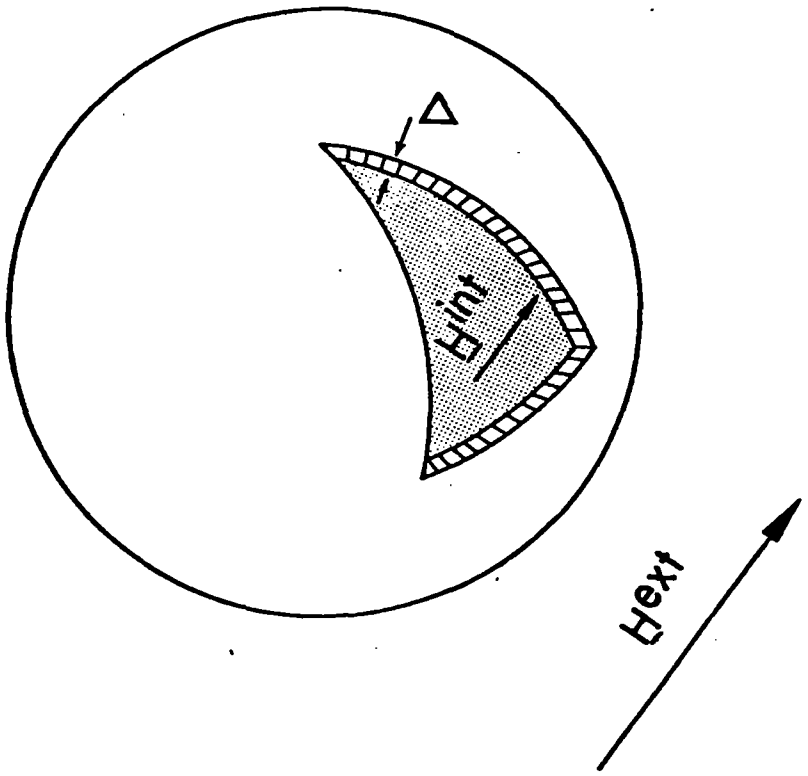

Figure 4. Shielding by a spherical shell with inner radius r, conductivity σ, and permeability μ.

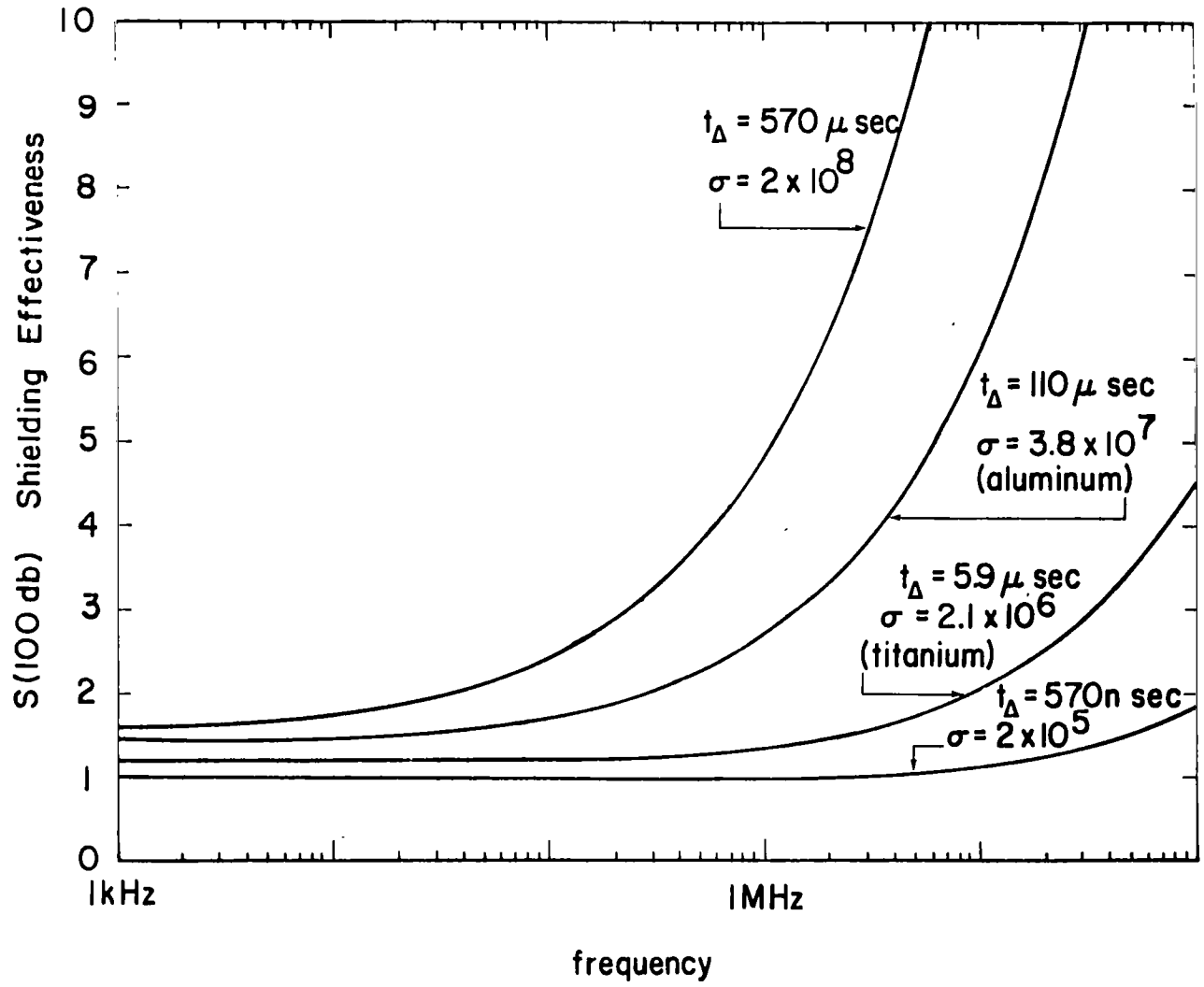

Figure 5(a). Single-plate shielding effectiveness with $\Delta = 1.5$ mm .

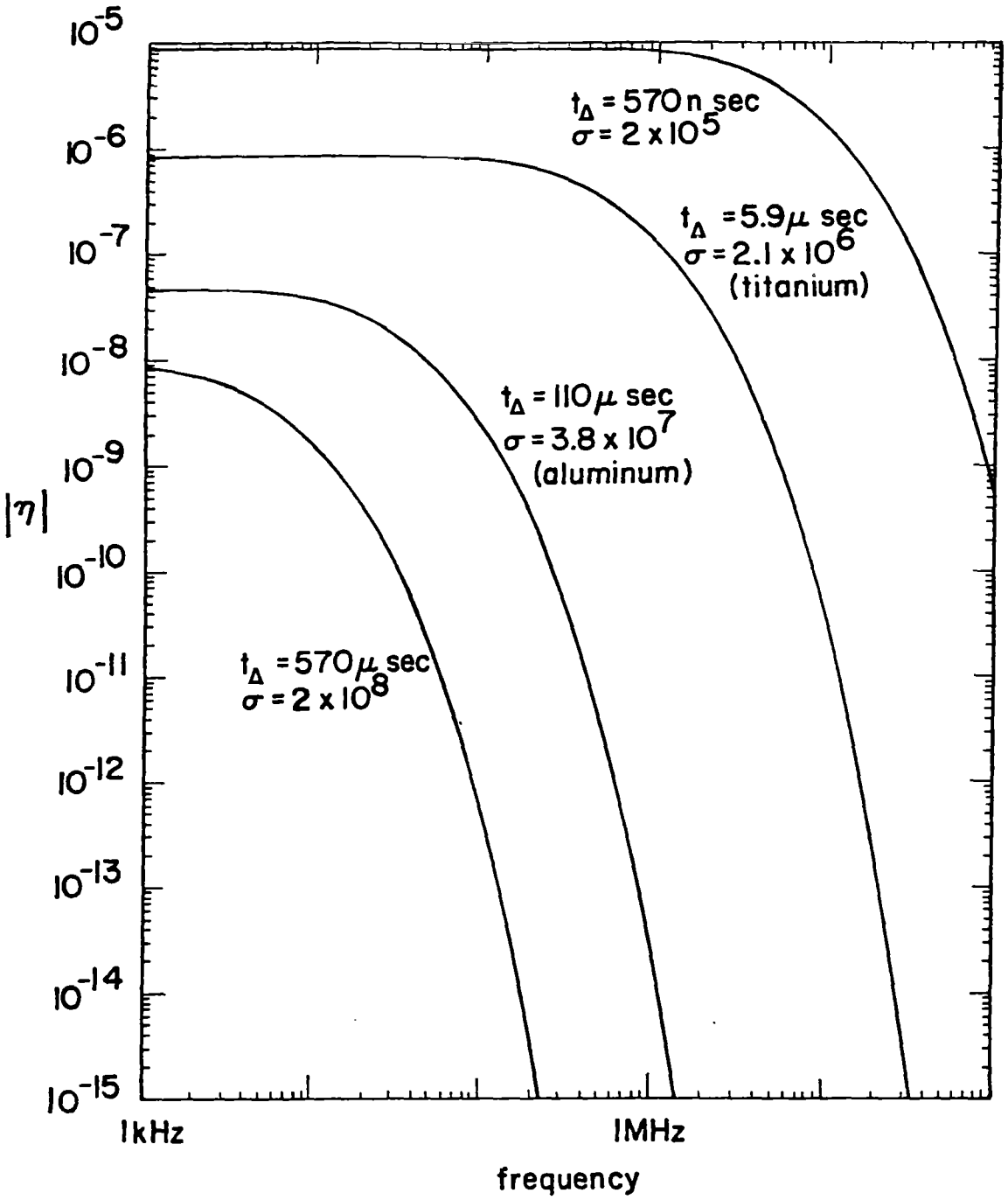

Figure 5(b). Single-plate transfer function with $\Delta = 1.5$ mm .

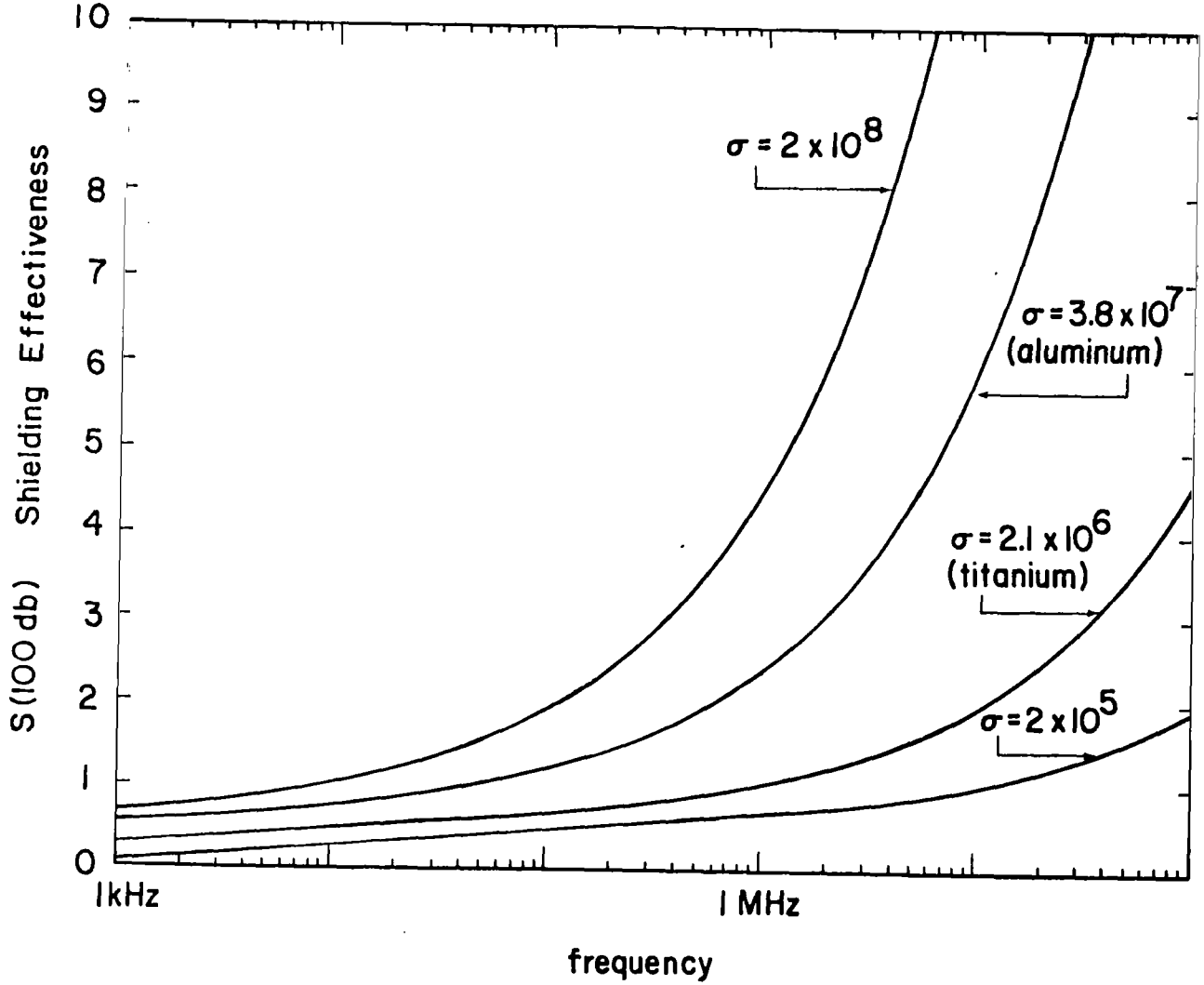

Figure 6(a). Enclosure shielding effectiveness of two parallel plates ($r = 1$ m), a cylindrical shell for transverse polarization ($r = 2$ m), and a spherical shell ($r = 3$ m). The wall thickness $\Delta = 1.5$ mm.

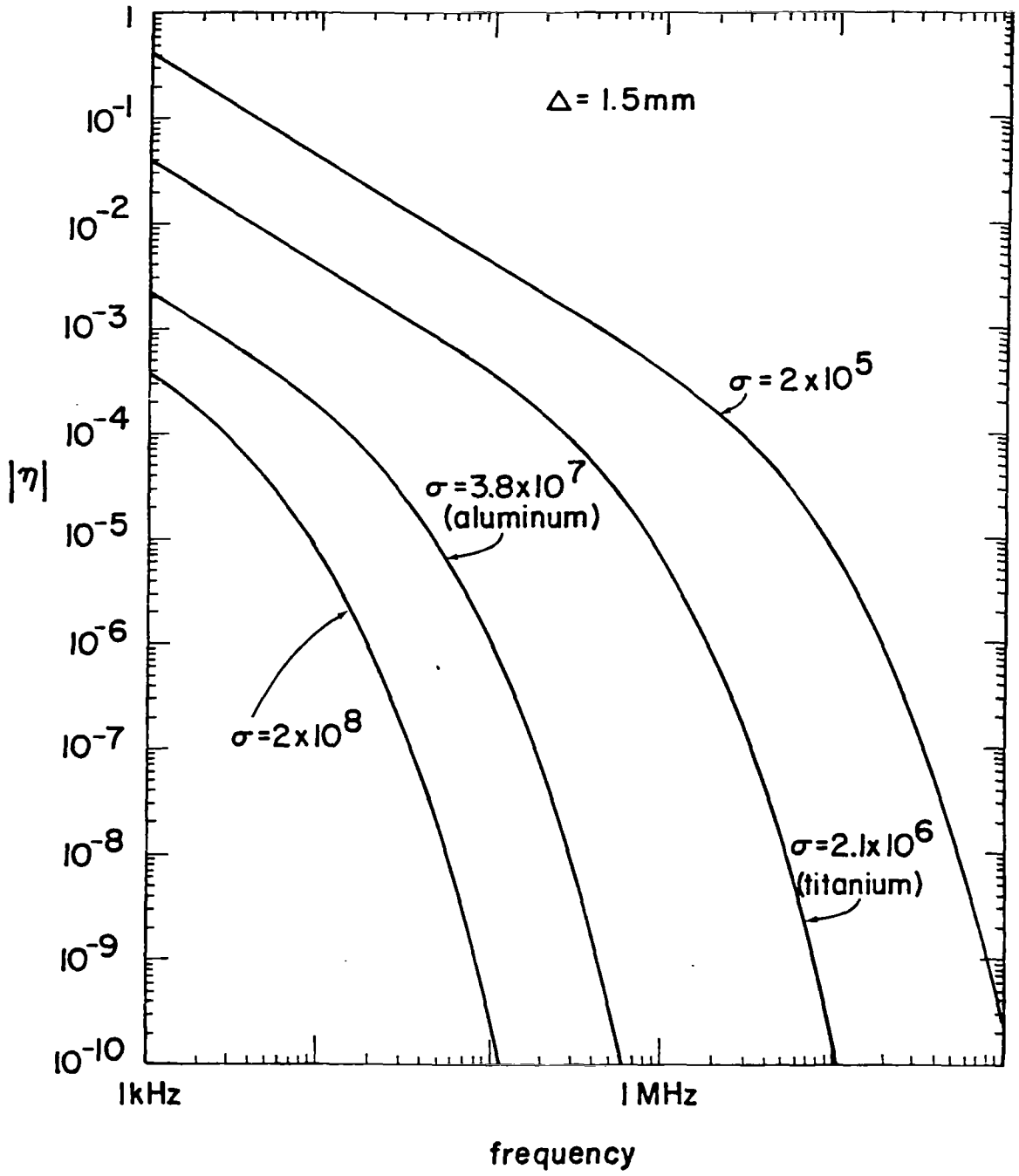

Figure 6(b). Enclosure transfer function.

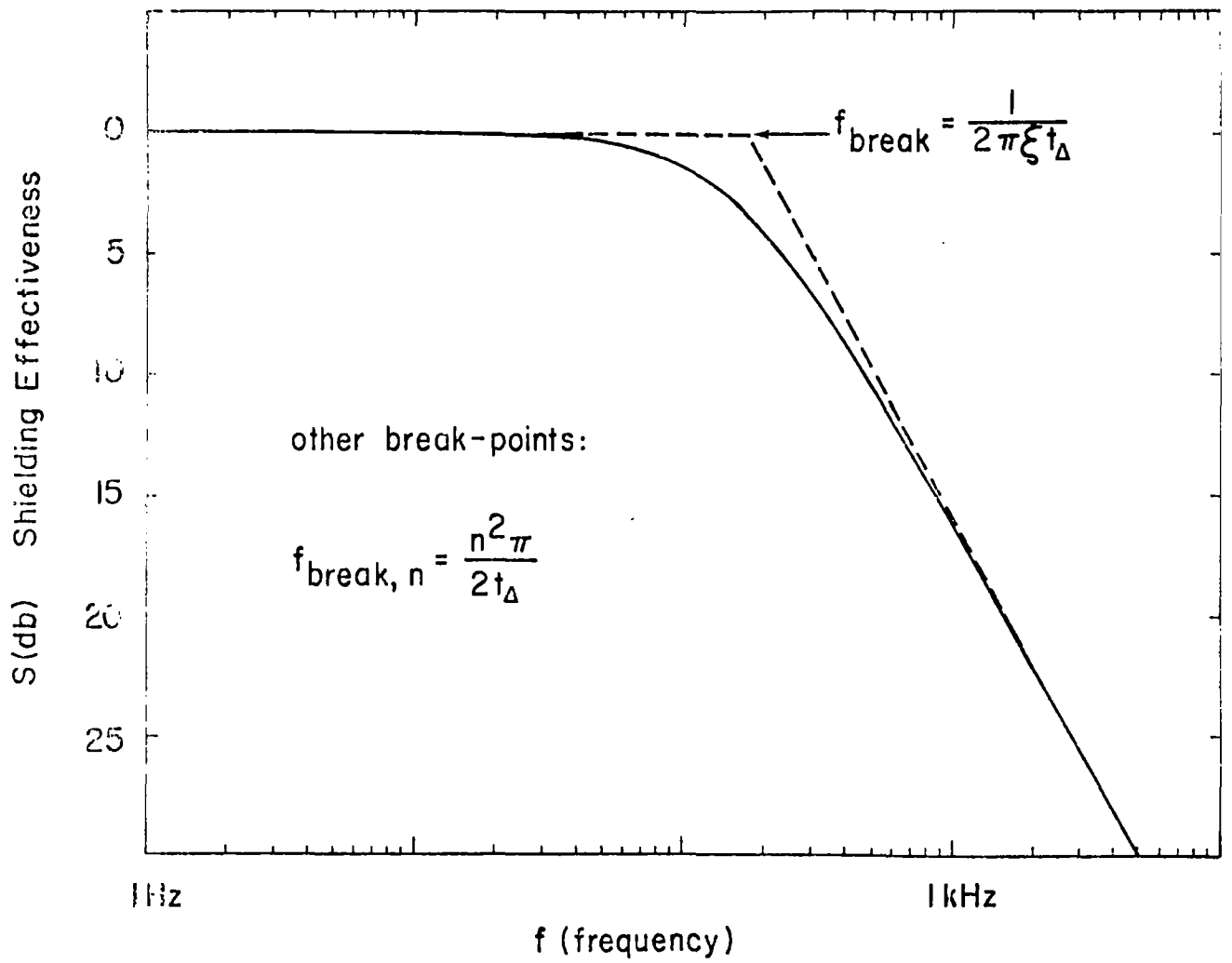

Figure 7. Low-frequency enclosure shielding effectiveness.

The first so-called frequency "break point" occurs at $f_b = (2\pi\xi t_\Delta)^{-1}$. Until this frequency, the shielding effectiveness is essentially zero. Afterward, the shielding effectiveness increases linearly with $\log_{10} f$; the slope is 20 db per decade of frequency. Figure 7 uses the values $\xi = 1000$ and $t_\Delta = 10^{-6}$ sec , but is easily scaled for other values of ξ and t_Δ . The position of the first break-point determines the late-time behavior of the interior field:

$$H^{int}(t) \approx e^{-2\pi f_b t} = e^{-t/(\xi t_\Delta)}$$

The other break-points occuring at higher frequencies are given by

$$f_{b,n} = \frac{n^2 \pi}{2t_\Delta} \quad , \qquad n = 1,2,3...$$

This expression will be derived later in connection with time-domain solutions.

B. Time Domain Solution

An impulse external magnetic field,

$$H^{ext}(t) = H_o \delta(t) \ ,$$

has a constant Laplace transform given by

$$H^{ext}(s) = H_o \ .$$

If one integrates both sides of the above time-domain equation, it is evident that

$$H_o = \int_{-\infty}^{\infty} H^{ext}(t)dt$$

Thus, if H^{ext} is a very short pulse compared to the response of the cavity, H_o can be introduced for the impulse equivalent strength of H^{ext} . The time

dependence of the internal magnetic field is then simply the inverse Laplace transform of the transfer function times the impulse equivalent strength:

$$H^{int}(t) = H_o L^{-1}[\eta(s)] ,$$

or in explicit form,

$$H^{int}(t) = \frac{H_o}{2\pi j} \int_{-j\infty+\alpha}^{j\infty+\alpha} \frac{e^{st} ds}{\cosh(st_\Delta)^{\frac{1}{2}} + [\xi_1 (st_\Delta)^{\frac{1}{2}} + \xi_2 (st_\Delta)^{-\frac{1}{2}}]\sinh(st_\Delta)^{\frac{1}{2}}} \qquad (5)$$

where ξ_1 and ξ_2 are dimensionless constants depending on the particular geometry (see equations 1 - 4), and α is any positive constant.

A representation of this integral which is especially useful for late times can be obtained by transforming s to z through $s = z^2/t_\Delta$. The integral then becomes

$$H^{int}(t) = \frac{2H_o}{t_\Delta} \frac{1}{2\pi j} \int_\Gamma \frac{z e^{z^2 t/t_\Delta} dz}{\cosh z + (\xi_1 z + \xi_2/z)\sinh z} \qquad (6)$$

where Γ is the hyperbolic contour illustrated in figure 8a.

The poles of the integrand in equation (6) are located along the imaginary axis in the z-plane at points $(z_n = jq_n)$ which satisfy the transcendental equation

$$\cot(q_n) = \xi_1 q_n - \xi_2/q_n \qquad (7)$$

Since the integrand is an odd function of z , the half of contour Γ below the real axis can be reflected through the origin. The two new halves can be joined along the real axis and at infinity in the upper quarter-plane without altering the integral, which results in contour Γ' . Cauchy's integral theorem yields the following infinite series results:

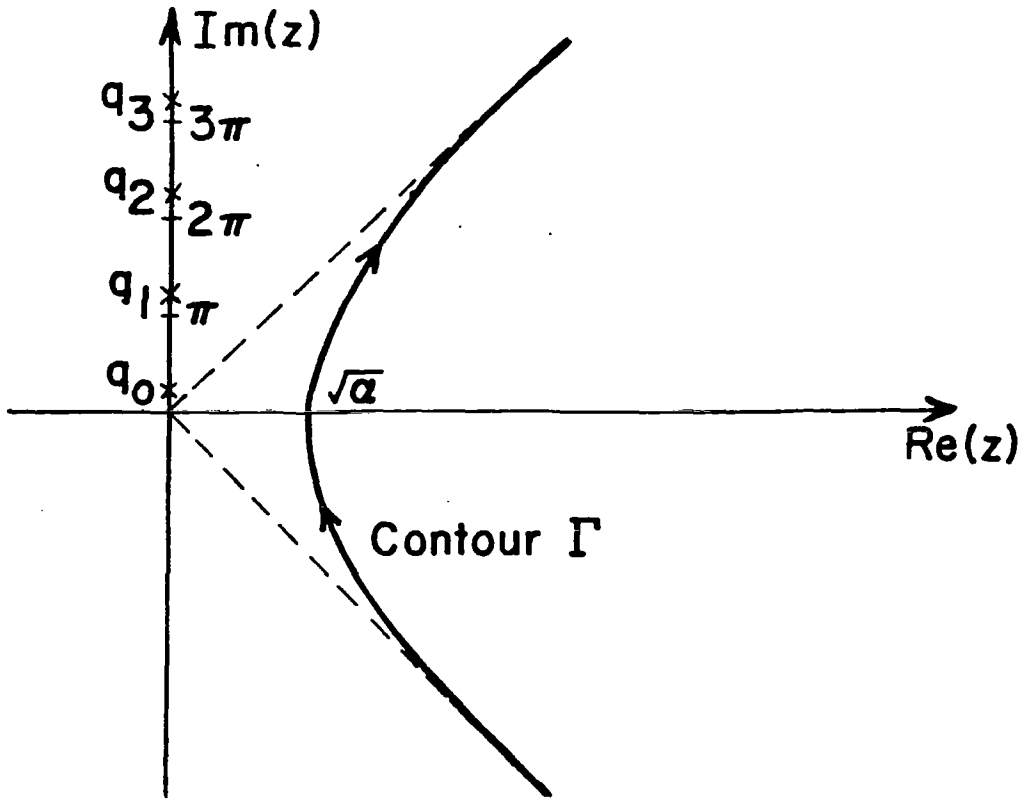

8(a)

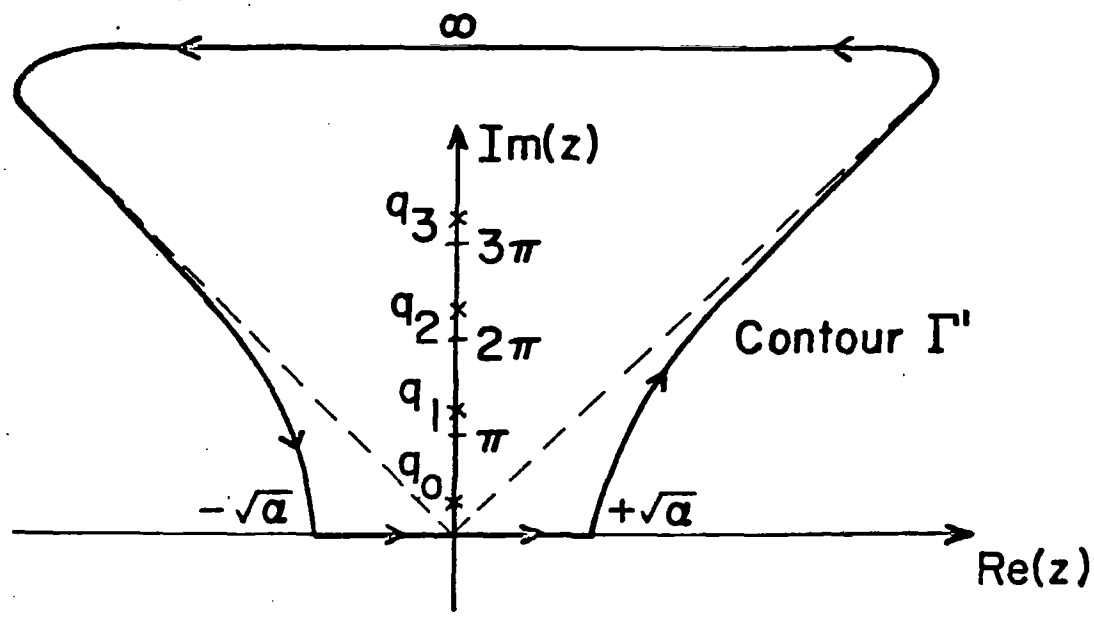

8(b)

Figure 8(a) - Contour Γ in the z-plane.
8(b) - Contour Γ' in the z-plane.

$$H^{int}(t) = \frac{2H_o}{t_\Delta} \sum_{n=0}^{\infty} \frac{q_n e^{-q_n^2 t/t_\Delta}}{\{1+\xi_1+\xi_1^2 q_n^2+[\xi_2+\xi_2^2]q_n^{-2}\}\sin q_n} \tag{8A}$$

$$\dot{H}^{int}(t) = -\frac{2H_o}{t_\Delta^2} \sum_{n=0}^{\infty} \frac{q_n^3 e^{-q_n^2 t/t_\Delta}}{\{1+\xi_1+\xi_1^2 q_n^2+[\xi_2+\xi_2^2]q_n^{-2}\}\sin q_n} \tag{8B}$$

Note that the sums run over all $q_n > 0$ satisfying equation (7). The series solutions of equation (8) are especially useful for late times because the exponential part ensures quick convergence when $t \gtrsim t_\Delta$. However, they are the exact solutions and converge formally for all $t > 0$. $\dot{H}^{int}(t)$ is directly proportional to the open-circuit voltage induced on a pickup loop inside the cavity.

A different approach must be used to find a good early-time representation. To do this, the contour parameter, α, is made arbitrarily large. Then $\eta(s)$ can be expanded for large s:

$$\eta(s) = \frac{2e^{-(st_\Delta)^{1/2}}}{1+\xi_1(st_\Delta)^{1/2}+\xi_2(st_\Delta)^{-1/2}} \sum_{n=0}^{\infty} \left\{ \frac{e^{-2(st_\Delta)^{1/2}}[-1+\xi_1(st_\Delta)^{1/2}+\xi_2(st_\Delta)^{-1/2}]}{1+\xi_1(st_\Delta)^{1/2}+\xi_2(st_\Delta)^{-1/2}} \right\}^n$$

which leads to the following infinite series of inverse Laplace transformations:

$$H^{int}(t) = 2H_o \sum_{n=0}^{\infty} L^{-1}\left\{ \frac{e^{-(2n+1)(st_\Delta)^{1/2}}[-1+\xi_1(st_\Delta)^{1/2}+\xi_2(st_\Delta)^{-1/2}]^n}{[1+\xi_1(st_\Delta)^{1/2}+\xi_2(st_\Delta)^{-1/2}]^{n+1}} \right\} \tag{9}$$

This series is not convenient to use in itself, but it leads to simple approximate expressions of the early-time solutions for the cases of interest, as will be seen below.

C. Explicit Approximate Solutions

Explicit approximate solutions for early times and late times can be

developed from equations (7) - (9) for the four canonical cases of interest [equations (1) - (4)].

C.1 Single Plate Geometry

For the single plate, $\xi_1 = 0$ and $\xi_2 = Z_o/R >> 1$ in equations (7) - (9). The late-time approximate solution can be obtained from equations (7) and (8A). The poles, q_n, are solutions of

$$\cot q_n = - (Z_o/R) q_n^{-1} \tag{10}$$

Since $Z_o/R >> 1$, the solutions are

$$q_n = n\pi - \varepsilon_n , \qquad n = 1,2,3,\ldots ,$$

where $0 < \varepsilon_n << 1$. The sine of q_n is approximately

$$\sin(q_n) \approx (-1)^{n+1} n\pi R/Z_o .$$

Of course, eventually the right-hand side of equation (10) will no longer be large as q_n increases, but the first several roots will be sufficient to give a good late-time representation. Substituting the approximate expressions for q_n and $\sin q_n$ in equation (8A) and taking the first three terms* , one obtains

$$H^{int}(t) \approx \frac{2\pi^2 H_o R}{t_\Delta Z_o} \left(e^{-\pi^2 t/t_\Delta} - 4e^{-4\pi^2 t/t_\Delta} + 9e^{-9\pi^2 t/t_\Delta} \right), \quad (t \geq t_\Delta/20) . \tag{11}$$

---

* The second and third terms are included to provide a better match with the early-time solution and can be neglected for $t \geq t_\Delta$.

The early-time approximate solution for a single plate is found by evaluating the first term in the infinite series of inverse Laplace transformation as given by equation (9) for $\xi_1 = 0$ and $\xi_2 = Z_o/R$:

$$H^{int}(t) \approx 2H_o L^{-1}\left[\frac{e^{-(st_\Delta)^{1/2}}}{1 + (Z_o/R)(st_\Delta)^{-1/2}}\right], \qquad (t << t_\Delta) .$$

This inverse Laplace transform is listed in standard mathematical tables [ref. 5]. The result is

$$H^{int}(t) \approx \frac{2H_o}{t_\Delta}\left\{\frac{t_\Delta}{\sqrt{\pi}\, t}\left[\frac{1}{2}\left(\frac{t_\Delta}{t}\right)^{1/2} - \frac{Z_o}{R}\left(\frac{t}{t_\Delta}\right)^{1/2}\right]e^{-t_\Delta/(4t)}\right. \tag{12}$$

$$\left. + \left(\frac{Z_o}{R}\right)^2 e^{[Z_o/R + (Z_o/R)^2(t/t_\Delta)]}\, \mathrm{erfc}\left[\frac{1}{2}\left(\frac{t_\Delta}{t}\right)^{1/2} + \frac{Z_o}{R}\left(\frac{t}{t_\Delta}\right)^{1/2}\right]\right\}$$

Since $t << t_\Delta$, the argument of erfc in equation (12) is large. A good approximation of erfc(x) when x is large is

$$\mathrm{erfc}(x) \approx \frac{e^{-x^2}}{\sqrt{\pi}\, x}$$

The early-time approximation then becomes

$$H^{int}(t) \approx \frac{2H_o e^{-t_\Delta/4t}}{\sqrt{\pi}\, t_\Delta}\left\{\frac{1}{2}\left(\frac{t}{t_\Delta}\right)^{-3/2} - \frac{Z_o}{R}\left(\frac{t}{t_\Delta}\right)^{-1/2}\right.$$

$$\left. + \left(\frac{Z_o}{R}\right)^2\left[\frac{1}{2}\left(\frac{t}{t_\Delta}\right)^{-1/2} + \left(\frac{Z_o}{R}\right)\left(\frac{t}{t_\Delta}\right)^{1/2}\right]^{-1}\right\}$$

This result is in need of further simplification. Since $Z_o/R >> 1$ for all practical metal skin panels, $[\frac{1}{2}(t/t_\Delta)^{-1/2} + (Z_o/R)(t/t_\Delta)^{1/2}]^{-1}$ can be expanded about the second term as long as $(t/t_\Delta) > \frac{1}{2} R/Z_o$, which holds for all but

the very earliest times (when the internal field is negligible anyway). The simplified early-time internal field is

$$H^{int}(t) \approx \frac{H_o e^{-t_\Delta/(4t)}}{\sqrt{\pi}\, t_\Delta} \left(\frac{R}{Z_o}\right)\left(\frac{t_\Delta}{t}\right)^{5/2} , \qquad (t \le t_\Delta/20) . \tag{13}$$

Figure 9 is a plot of $H^{int}(t)$ versus t, taken for the cases for which $Z_o/R >> 1$. The three curves represent the early-time [equation (13)], late-time [equation (11)], and exact [equation (8A)] solutions. From the graph, one can see that the transition from the early- to late-time approximation should occur near $t = t_\Delta/20$.

C.2 Enclosure Geometries

Explicit early-time and late-time approximations can be obtained for the enclosure geometries in a similar manner. In all enclosure cases commonly found onboard an aircraft, $\xi_1 >> 1 >> \xi_2$ in equations (7) - (9). The locations of the poles of the transfer function will therefore depend almost entirely on ξ_1 [recall equation (7)]. The roots needed for the late-time representation satisfy

$$\cot q_n = \xi_1 q_n , \qquad \xi_1 >> 1 . \tag{14}$$

The solutions are

$$q_n = n\pi + \varepsilon_n , \qquad n = 0,1,2,\ldots , \qquad 0 < \varepsilon_n << 1 .$$

The values of ε_n are insignificant for all but the 0^{th} root. For that root,

$$q_o = \varepsilon_o \approx \xi_1^{-1/2} .$$

The first three terms* of the infinite series in equation (8A) give the late-time

* Again, the second and third terms are included to provide a better match with the early-time approximation and can be neglected when $t > t_\Delta$.

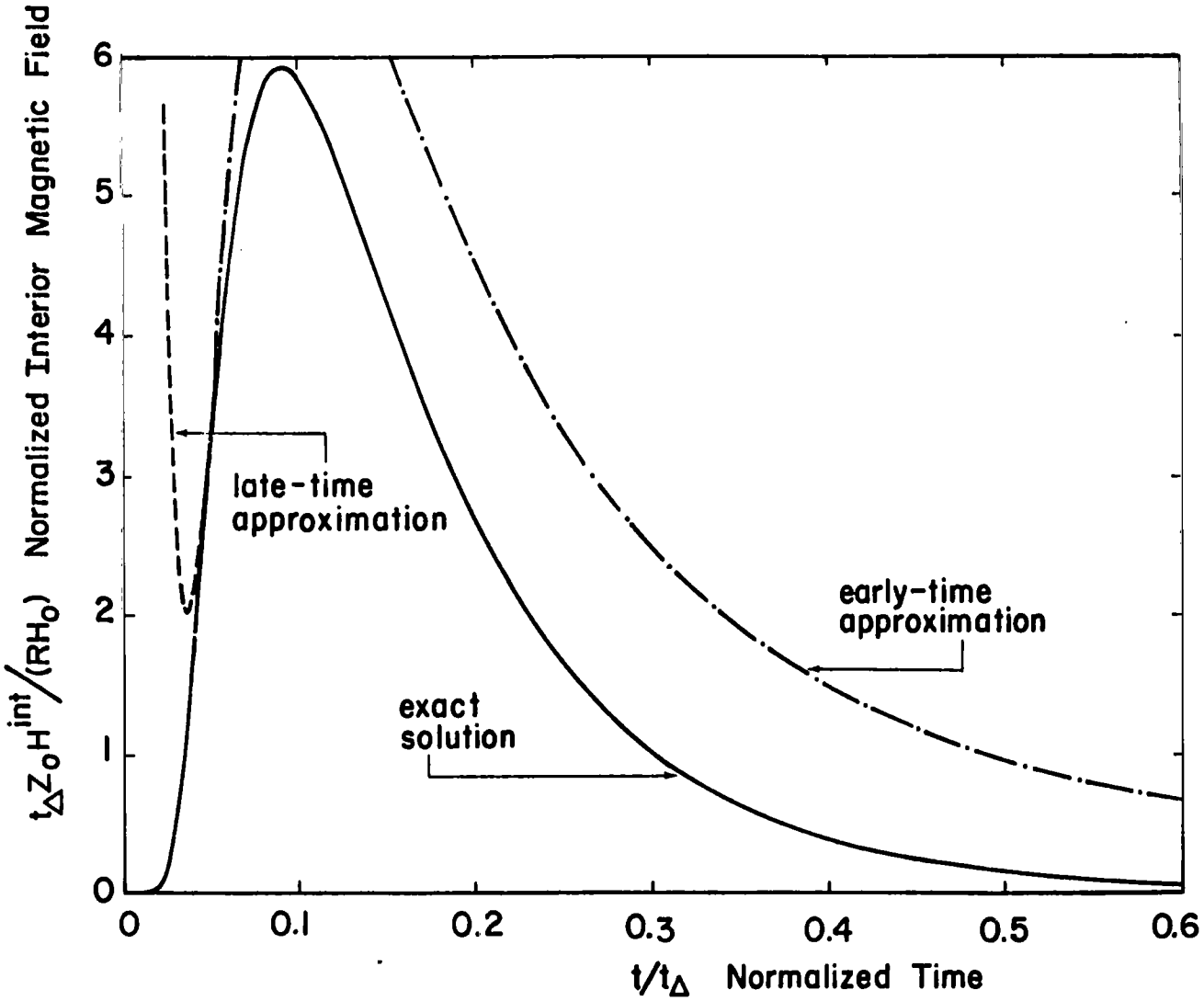

Figure 9. Single-plate impulse response.

approximation:

$$H^{int}(t) \approx \frac{H_o}{\xi_1 t_\Delta}\left(e^{-t/(\xi_1 t_\Delta)} - 2e^{-\pi^2 t/t_\Delta} + 2e^{-4\pi^2 t/t_\Delta}\right), \quad (t \geq t_\Delta/10) \ . \qquad (15)$$

The early-time approximation for the enclosure geometries can be calculated from the first term of the infinite series of inverse Laplace transforms in equation (9); that is to say, one must evaluate

$$H^{int}(t) \approx 2H_o L^{-1}\left[\frac{e^{-(st_\Delta)^{1/2}}}{1+\xi_1(st_\Delta)^{1/2}+\xi_2(st_\Delta)^{-1/2}}\right]$$

When the contour is "pushed" to the far right in the s-plane to obtain the early-time representation, $(st_\Delta)^{-1/2}$ will be small compared with unity and in all practical aircraft cavities, ξ_2 is either small or zero. Thus, the ξ_2 term can be neglected and one is left with

$$H^{int}(t) \approx 2H_o L^{-1}\left[\frac{e^{-(st_\Delta)^{1/2}}}{1+\xi_1(st_\Delta)^{1/2}}\right].$$

This inverse Laplace transform is available in mathematical tables [ref. 5] ; the result is

$$H^{int}(t) \approx \frac{2H_o e^{-t_\Delta/(4t)}}{\sqrt{\pi}\,\xi_1 t_\Delta}\left(\frac{t_\Delta}{t}\right)^{1/2} - \frac{2H_o e^{[\xi_1^{-1}+t/(\xi_1^2 t_\Delta)]}}{\xi_1^2 t_\Delta}\,\mathrm{erfc}\left[\frac{1}{2}\left(\frac{t_\Delta}{t}\right)^{1/2} + \frac{1}{\xi_1}\left(\frac{t}{t_\Delta}\right)^{1/2}\right] \qquad (16)$$

When the same sort of expansion used for the single-plate early-time representation is performed on erfc in equation (16), it is seen that the contribution of the second term is negligible. The early-time approximation is then simply

$$H^{int}(t) \approx \frac{2H_o e^{-t_\Delta/(4t)}}{\sqrt{\pi}\,\xi_1 t_\Delta}\left(\frac{t_\Delta}{t}\right)^{1/2}, \qquad (t \leq t_\Delta/10) \; . \tag{17}$$

Figure 10 is a plot of the early-time [equation (17)], late-time [equation (15)], and exact [equation (8A)] solutions for enclosure geometries, for the cases in which the wall thickness is small compared with the cavity dimensions and the relative permeability is one (ξ_1 is large). For $t > t_\Delta/10$, the late-time and exact solutions are indistinguishable, both exhibiting an exponential decay time equal to $\xi_1 t_\Delta$. The value of ξ_1 depends on the geometry of the enclosure, as will be discussed below.

Figures 9 and 10 can be regarded as "universal curves," because the time axes are scaled by the diffusion time, t_Δ, and the magnetic field strength axes are scaled by the reciprocal of the appropriate constant, ξ_1 or ξ_2, depending on the geometry. These curves fail to be "universal" only when ξ_1 (or ξ_2) fails to be large compared with unity, i.e., only when the wall thickness is comparable to the dimensions of the cavity (or the dc resistance is high). Figures 11 and 12 illustrate this effect for various values of ξ_1 or ξ_2, where H^{int} is plotted versus t using the exact infinite series. For the enclosure geometries, there is a strong dependence on shape (and polarization) which is seen when ξ_1 is small but not when ξ_1 is large.

Since figures 9 and 10 are universal curves, the parameters that characterize the important features of the penetrant pulse can be read from them directly. These parameters are summarized in table I, with ξ replacing ξ_1.

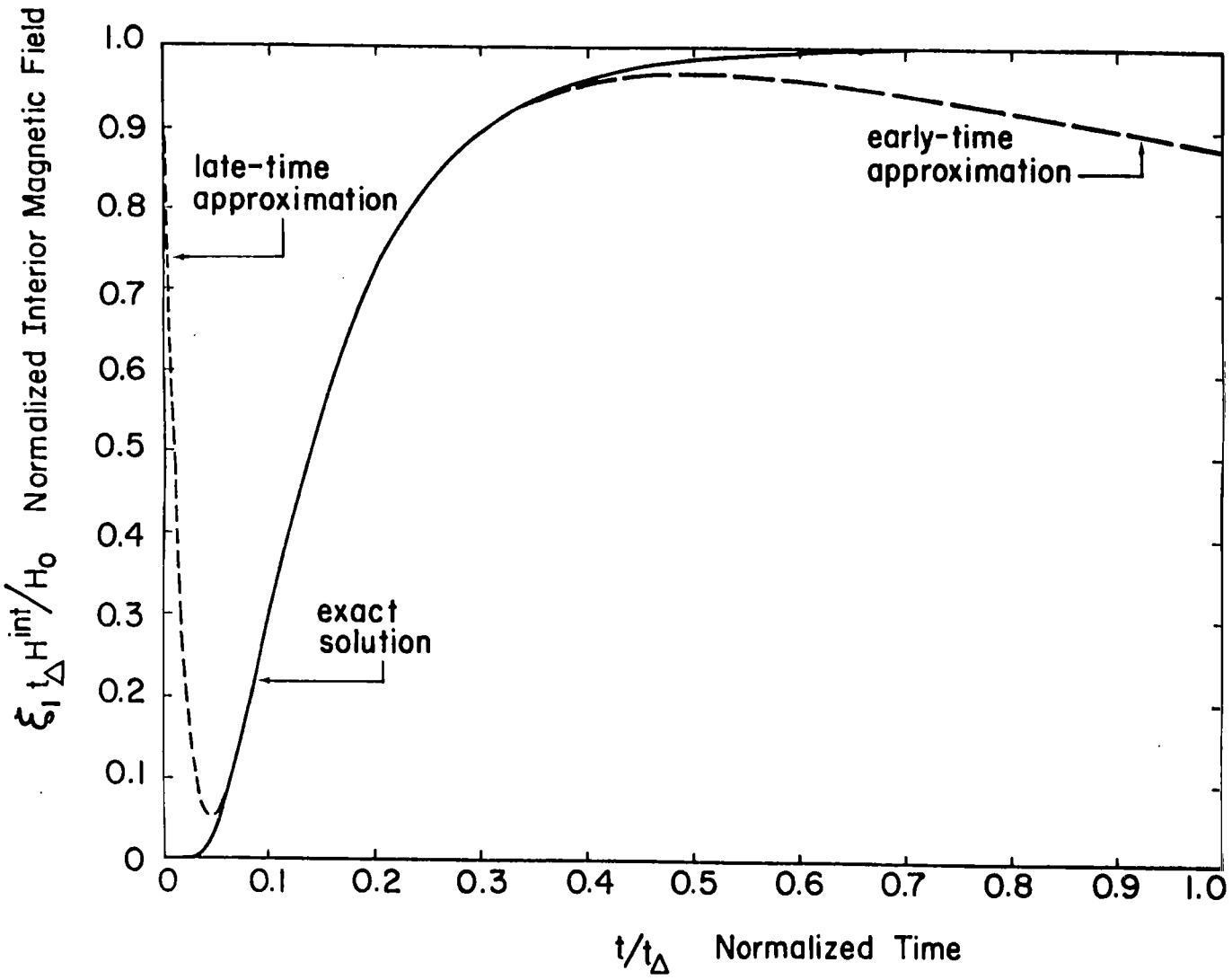

Figure 10. Enclosure impulse response ($\xi_1 \geq 100$) for two parallel plates ($\xi_1 = r/\Delta$), a cylindrical shell ($\xi_1 = r/2\Delta$), and a spherical shell ($\xi_1 = r/3\Delta$).

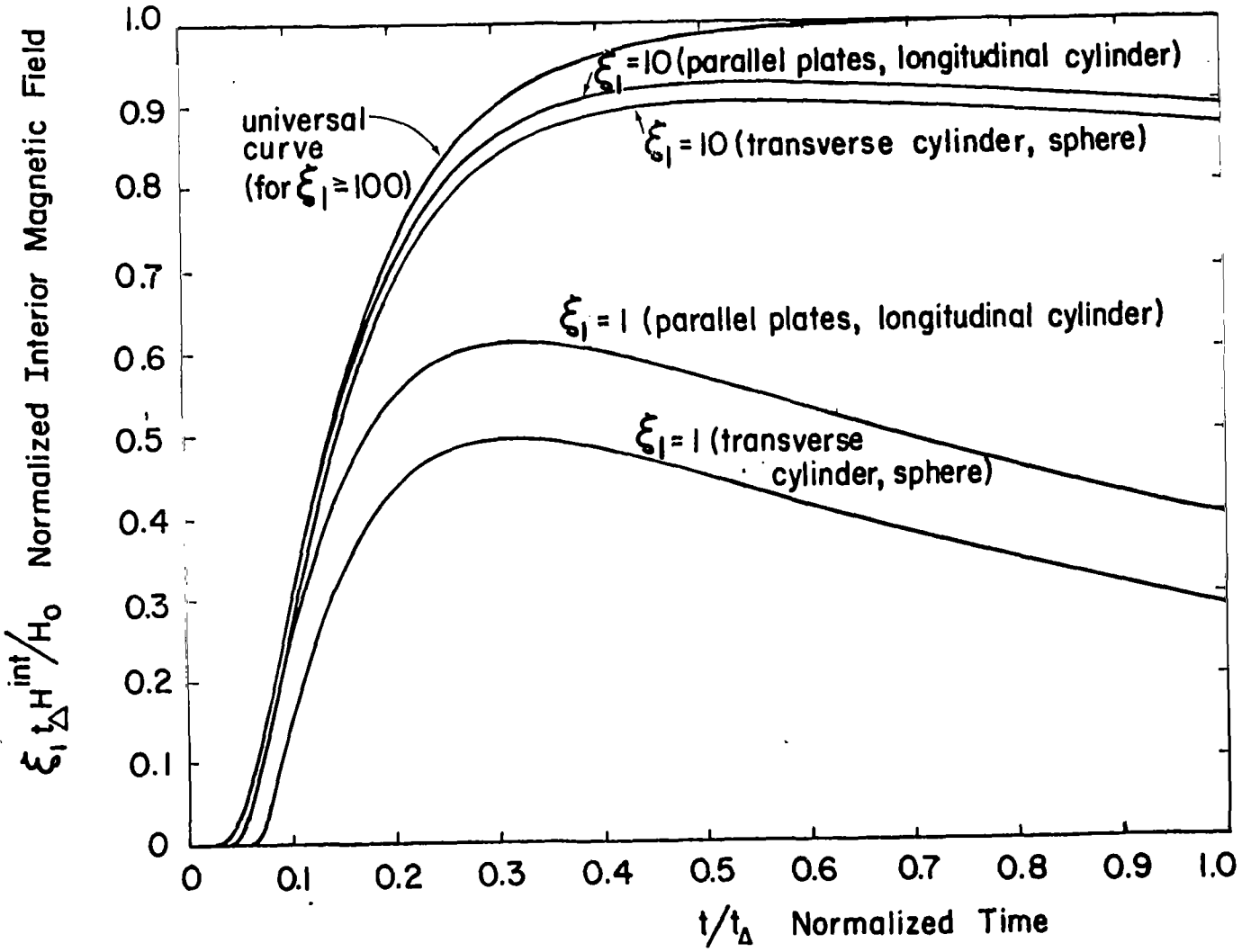

Figure 11. Effect of geometry on enclosure response.

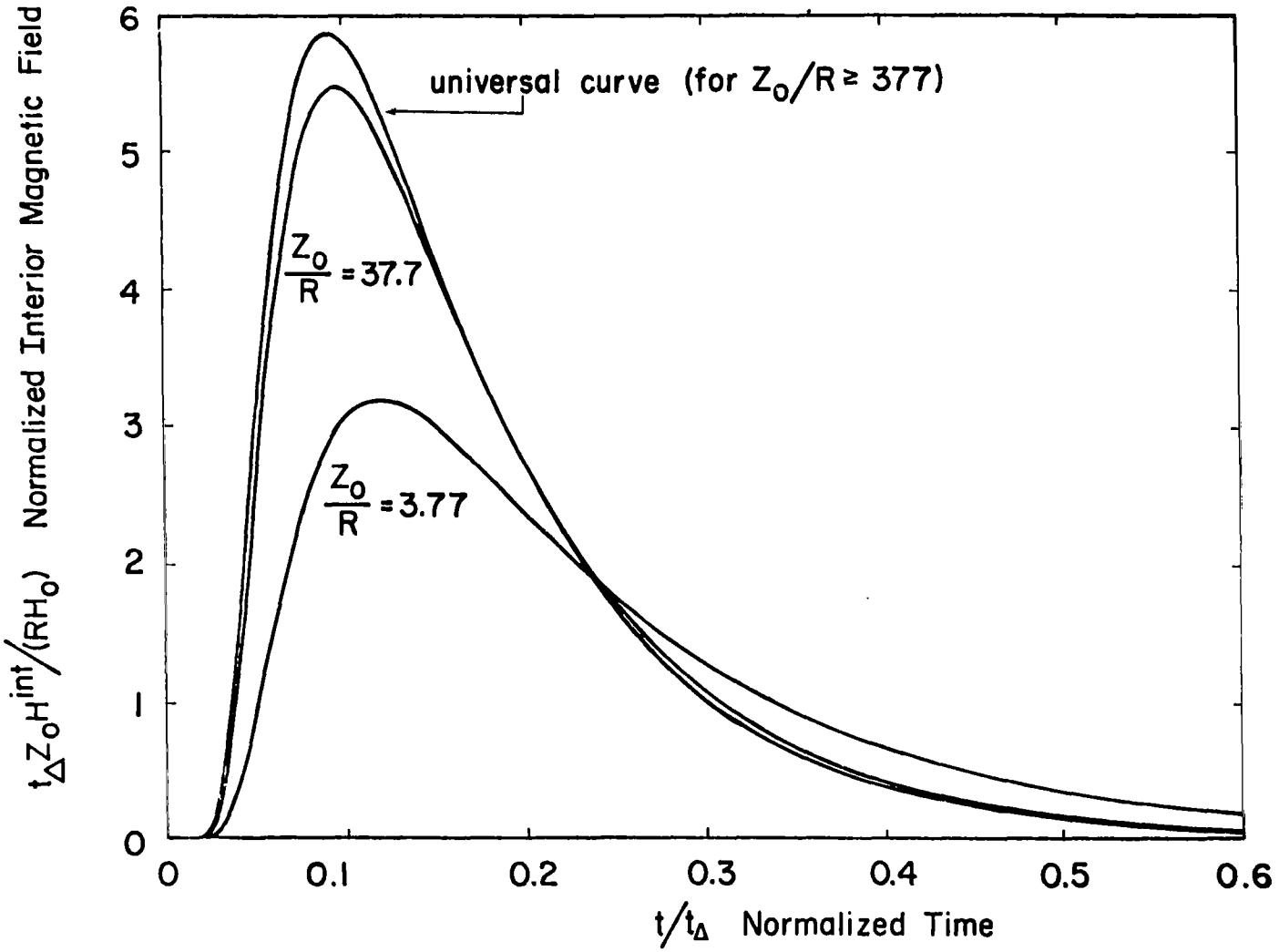

Figure 12. Effect of dc skin resistance on single-plate response.

Table I. Engineering Parameters of the Penetrant Pulse

Geometry	ξ	H^{int} (peak)	$\dot{H}^{int}$ (peak)	Rise Time (10 - 90%)	Decay Time (1/e)
Single plate	$\frac{Z_o}{R}$	$\frac{6\ H_o}{\xi t_\Delta}$	$\frac{120\ H_o}{\xi t_\Delta^2}$	$\frac{t_\Delta}{20}$	$\frac{t_\Delta}{\pi^2}$
Parallel plates	$\frac{\mu_o r}{\mu\Delta}$	$\frac{H_o}{\xi t_\Delta}$	$\frac{6\ H_o}{\xi t_\Delta^2}$	$\frac{t_\Delta}{4}$	ξt_Δ
Cylinder	$\frac{\mu_o r}{2\mu\Delta}$	$\frac{H_o}{\xi t_\Delta}$	$\frac{6\ H_o}{\xi t_\Delta^2}$	$\frac{t_\Delta}{4}$	ξt_Δ
Sphere	$\frac{\mu_o r}{3\mu\Delta}$	$\frac{H_o}{\xi t_\Delta}$	$\frac{6\ H_o}{\xi t_\Delta^2}$	$\frac{t_\Delta}{4}$	ξt_Δ

D. Generalization to Arbitrary Enclosure Geometry

The results of figures 9 and 10 are suggestive of the existence of a general formula which is valid for arbitrary cavity geometry when the wall is thin compared to a typical cavity dimension. It can be seen from figure 11 that detailed geometrical differences become less important as the ratio of cavity size to wall thickness becomes large. However, there is a factor of one, two, or three that needs to be explained in the overall results, depending on whether the geometry is one-, two-, or three-dimensional.

The factor of one, two, or three suggests a relationship with the volume-to-surface ratio. As evident from table I, two parameters, namely, the diffusion time t_Δ and the decay time t_d, completely determine the other engineering parameters. The diffusion time is easily calculated for any

cavity from a knowledge of the wall permeability, conductivity, and thickness (recall the definition of t_Δ) . The decay time can be computed for a cavity by a simple circuit analogy. There is a dc skin resistance given by $R = (\sigma\Delta)^{-1}$, which is not shape-dependent. Currents induced in the wall will decay through resistive heating. These same currents are presented with an effective inductance inside the cavity given by

$$L = \mu_o V/S \ .$$

The analogy is a simple R-L circuit, and the decay time is given by

$$t_d = L/R \ .$$

The constant, ξ , is simply the ratio of t_d to t_Δ , or

$$\xi = \mu_o V/(\mu\Delta S) \tag{18}$$

This result allows calculation of the engineering parameters of an interior pulse in arbitrarily-shaped cavities. In terms of ξ and t_Δ ,

$$H^{int}(peak) = \frac{H_o}{\xi t_\Delta} \tag{19A}$$

$$\dot{H}^{int}(peak) = \frac{6\ H_o}{\xi t_\Delta^2} \tag{19B}$$

$$t_r = \text{Rise Time } (10-90\%) = \frac{t_\Delta}{4} \tag{19C}$$

$$t_d = \text{Decay Time } (1/e) = \xi t_\Delta \ , \tag{19D}$$

provided $\xi >> 1$.

III. SUMMARY AND CONCLUSION

The approximate expressions derived in section II provide a convenient method for the estimation of the EMP diffused penetrant magnetic field in many aircraft configurations, such as cockpits, weapons bays, avionics bays, and other metallic cavities. The approximate expressions assume an impulse incident field, and so they are applicable as long as the diffusion time, t_Δ , is much longer than the pulse width of the incident EMP. The pulse width of a typical high-altitude EMP is on the order of hundreds of nanoseconds, while an aluminum skin panel of one millimeter in thickness has a diffusion time of about fifty microseconds, and so the EMP is effectively an impulse for typical aircraft cavities.

To summarize the important results, it is convenient to define the following parameters:

Δ = thickness of skin panel

σ = conductivity of skin panel

$\mu_o = 4\pi \times 10^{-7}$ henries per meter = free-space permeability

μ = permeability of skin panel

$t_\Delta = \mu\sigma\Delta^2$ = diffusion time constant of skin panel

$Z_o = 377\ \Omega$ = free-space impedance

$R = (\sigma\Delta)^{-1}$ = dc skin panel resistence

V = cavity volume

S = cavity surface area

$L = \mu_o V/S$ = cavity inductance

$$\xi = \begin{cases} Z_o/R & \text{(single skin panel)} \\ \mu_o V/(\mu\Delta S) = L/(Rt_\Delta) & \text{(cavities)} \end{cases}$$

$$H_o = \int_{-\infty}^{\infty} H^{ext}(t)dt = \text{equivalent impulse strength}$$

The penetrant pulse is given (to 0.1% accuracy for the canonical cases) by the formulas in table II. These approximate equations are valid as long as $\xi >> 1$ (high conductivity in thin walls), $\varepsilon\omega << \sigma$ (Kaden's diffusion approximation), and $\lambda = c/f >> r$ (wavelength of the incident field at frequencies of interest greater than the size of the configuration). These assumptions hold for all metallic skin panels and metallic aircraft configurations for the important portion of a typical EMP spectrum. Figures 9 and 10 are graphical representations of the equations in table II.

It should be emphasized that the single-plate shielding effectiveness is not in general a relevant parameter to use in the calculation of the magnetic field diffused through a metal skin panel and into a typical aircraft cavity [ref. 6]. It is seen from figures 5 and 6 that low-frequency shielding effectiveness is much greater for a single plate than for an enclosure constructed of skin panels identical to the single plate. Figure 13 is a direct comparison of the single-plate and enclosure shielding effectiveness for aluminum and titanium skin panels with $\Delta = 1.5$ mm (0.06") and V/S = 1 meter. Because of the great difference between the single-plate and cavity cases, it is always necessary to know the geometry of the aircraft configuration, as well as the skin-panel parameters, when the diffused penetrant magnetic field is to be calculated.

In ref. 4 the engineering results presented in equations (18) - (19D) will be applied to particular aircraft cavities of interest: the B-1 central avionics bay, the B-1 forward weapons bay, the EC-135 cockpit, the EC-135 fuselage, and the E-4 cockpit.

Table II. Engineering Formulas for the Penetrant Pulse

Single plate

$$t \le t_\Delta/20 \qquad H^{int}(t) = \frac{H_o e^{-t_\Delta/(4t)}}{\sqrt{\pi}\, t_\Delta}\left(\frac{R}{Z_o}\right)\left(\frac{t_\Delta}{t}\right)^{5/2}$$

$$t \ge t_\Delta/20 \qquad H^{int}(t) = \frac{2\pi^2 H_o}{t_\Delta}\left(\frac{R}{Z_o}\right)\left[e^{-\pi^2 t/t_\Delta} - 4e^{-4\pi^2 t/t_\Delta} + 9e^{-9\pi^2 t/t_\Delta}\right]$$

Enclosures

$$t \le t_\Delta/10 \qquad H^{int}(t) = \frac{2H_o e^{-t_\Delta/(4t)}}{\sqrt{\pi}\ \xi\, t_\Delta}\left(\frac{t_\Delta}{t}\right)^{1/2}$$

$$t \ge t_\Delta/10 \qquad H^{int}(t) = \frac{H_o}{\xi t_\Delta}\left[e^{-t/(\xi t_\Delta)} - 2e^{-\pi^2 t/t_\Delta} + 2e^{-4\pi^2 t/t_\Delta}\right]$$

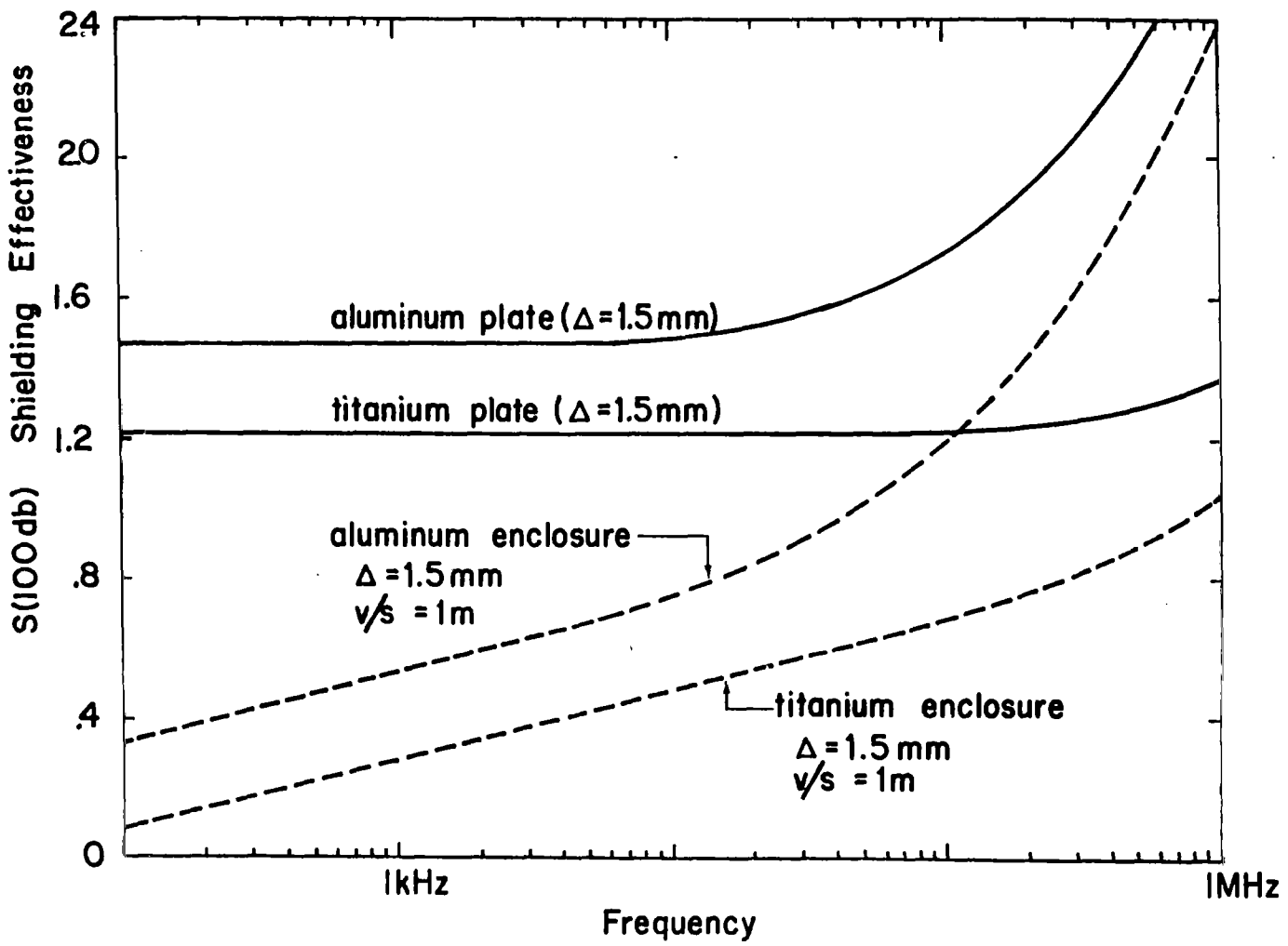

Figure 13. Single-plate and enclosure shielding effectiveness.

REFERENCES

[1] V.A. Ambarzumian, "Diffuse Reflection of Light by a Foggy Medium," Comptes Rendus (Doklady) de L'Academy des Sciences de l'URSS, vol. 38, pp. 229 - 232, 1943.

[2] H. Kaden, Wirbelströme und Schirmung in der Nachrichtentechnik (Springer-Verlag, Berlin, 1959).

[3] C.E. Baum, Air Force Weapons Laboratory, Albuquerque, New Mexico (private communication).

[4] G. Bedrosian and K.S.H. Lee, AIP Memos, Memo 2, Air Force Weapons Laboratory, Kirtland AFB, N.M., August 1976.

[5] A. Erdélyi (Ed.) et. al., Tables of Integral Transforms (McGraw-Hill, New York, 1954).

[6] R.W. Latham and K.S.H. Lee, "Theory of Inductive Shielding," Interaction Notes, Note 12, Air Force Weapons Laboratory, Kirtland AFB, N.M., March 1968.